A Midlatitude Cirrus Cloud Climatology from the Facility for Atmospheric Remote Sensing. Part I: Macrophysical and Synoptic Properties

KENNETH SASSEN

Meteorology Department, University of Utah, Salt Lake City, Utah

JAMES R. CAMPBELL

Science Systems and Applications, Inc., NASA Goddard Space Flight Center, Greenbelt, Maryland

(Manuscript received 5 January 2000, in final form 26 June 2000)

ABSTRACT

A uniquely extensive high cloud dataset has been collected from the University of Utah Facility for Atmospheric Remote Sensing in support of the First (ISCCP) International Satellite Cloud Climatology Project Regional Experiment extended time observations satellite validation effort. Here in Part I of a series of papers examining the climatological properties of the cirrus clouds studied over Salt Lake City, Utah, ~2200 h of data collected from 1986–96 is used to create a subset of 1389 hourly polarization ruby (0.694 μm) lidar measurements of cloud layer heights. These data were obtained within ± 3 h of the local 0000 UTC National Weather Service radiosonde launches to provide reliable cloud temperature, pressure, and wind data. Future parts of this series will consider the inferred cirrus cloud microphysical and radiative properties.

In addition to describing the cirrus macrophysical properties in terms of their yearly, seasonal, and monthly means and variabilities, the synoptic weather patterns responsible for the cirrus are characterized. The strong linkage between cirrus and weather is controlled by upper-air circulations mainly related to seasonally persistent intermountain region ridge/trough systems. The cloud-top heights of cirrus usually associated with jet streams tend to approach the local tropopause, except during the summer season due to relatively weak monsoonal convective activity. Although a considerable degree of variability exists, 10-yr average values for cirrus cloud-base/top properties are 8.79/11.2 km, 336.3/240.2 mb, $-34.4°/-53.9°$C, 16.4/20.2 m s^{-1}, and 276.3°/275.7° wind direction. The average cirrus layer physical thickness for single and multiple layers is 1.81 km. Estimates of cloud optical thickness τ based on a ''thin'' (i.e., bluish) visual appearance suggest that $\tau \lesssim 0.3$ occur ~50% of the time for detected cirrus, implying that the cirrus in the region of study may be too tenuous to be effectively sampled using current satellite methods. The global representativeness of this extended cirrus cloud study is discussed.

1. Introduction

After decades of heightened scientific awareness of the importance of cirrus clouds to climate, it may still be questioned whether we have sufficiently enhanced our understanding of their properties to resolve key issues. Foremost, is the basic question of the net effect of cirrus clouds on the radiation balance of the earth–atmosphere system; that is, do they act to maintain our climate by the heating or the cooling of our planet on both regional and global scales (Liou 1986). Similarly, in view of the possibilities for human-induced climate change on societal timescales, the response of cirrus clouds to a changing Earth from such factors as greenhouse gas buildup and the contamination of the upper troposphere from increasing aircraft traffic, is still unknown. In effect, in a perturbing climate, will the induced changes in cirrus cloud properties enhance, oppose, or even negate the hypothesized global warming effect. Atmospheric responses to changes in cirrus properties may also contribute to affecting regional circulations and weather systems. Such considerations could have major implications for the conduct of human activities well into the future.

What is currently known of the climatic impact of cirrus has come from theoretical simulations based on idealized cloud macrophysical and microphysical inputs, and a number of radiative transfer approximations. The results imply that the dominance of infrared greenhouse warming versus solar albedo cooling depends sensitively on both the heights and microphysical compositions of the modeled cirrus. Cloud height has an obvious impact because spatially extensive high-altitude ''blankets'' display a pronounced effect at intercepting and ''trapping'' the warm terrestrial radiation emitted

Corresponding author address: Kenneth Sassen, 135 S. 1460 E., (819 WBB), University of Utah, Salt Lake City, UT 84112.
E-mail: ksassen@met.utah.edu

in combination from the ground and the underlying atmosphere. Thus, high tropical cirrus derived from deep convection above warm moist layers, for example, display the potential for being particularly effective greenhouse modulators. Conversely, lower cirrus over cold terrain could be more important in terms of albedo effects. This suggests that midlatitude cirrus may display radiative effects that vary with the season. The situation becomes even more convoluted in cases of multiple and broken cloud layers.

In addition to their macrophysical effects, cirrus cloud radiative effects can not be realistically evaluated without considering the precise nature of cloud microphysical content. A number of numerical studies have indicated that it is the cirrus ice crystal size distribution, or effective particle size, that is of paramount importance (e.g., Stephens et al. 1990; Takano and Liou 1995; Khvorostyanov and Sassen 1998). For a given set of environmental conditions, the imbalance between the greenhouse and albedo effects is a function of cirrus cloud particle size, ideally with the smaller particles giving rise to increased solar reflectances, versus the more active trapping of terrestrial radiation when larger cirrus cloud particles dominate.

It should not be overlooked, however, that cirrus clouds are the product of *weather processes* (Stone 1957), such that their occurrence and macrophysical properties will vary significantly over the globe. Weather is a regional phenomenon, and to understand cirrus climatic effects it is necessary to comprehend why cirrus occur regionally. Once generated, cirrus cloud systems can propagate over vast distances (Starr and Wiley 1990). Therefore, a major purpose of the current work is to define the conditions under which our varieties of midlatitude cirrus clouds were generated, for it is through this examination that the global representativeness of our findings, and those of other recent remote sensing high cloud studies, can be evaluated. For example, regional cirrus cloud lidar studies have been reported from such diverse localities as southern (midlatitude) and northern (subtropical) Australia (Platt et al. 1987), the western tropical Pacific (Platt et al. 1998; Sassen et al. 2000), and southern Japan (Imasu and Iwaska 1991). Although the appropriateness of the sampling procedures for determining cirrus cloud climatologies needs to be carefully considered [see Sassen (2001) and section 2a for our definition of cirrus clouds], it is clear that the findings from a single locality cannot be regarded as being globally representative. We stress that this regional variability in cirrus properties is critical to understanding their global effects.

Recognizing that more observational studies of cirrus clouds are needed to lessen the uncertainty in the climatic role played by cirrus, recent comprehensive cirrus cloud studies employing remote sensors and high-altitude aircraft have been conducted in connection with the First International Satellite Cloud Climatology Project (ISCCP) Regional Experiment (FIRE) field campaigns (Cox et al. 1987), the Atmospheric Radiation Measurement (ARM) Program (Stokes and Schwartz 1994), and the International Cirrus Experiment (ICE) (Raschke et al. 1990). As part of our participation in Project FIRE, we began in 1987 supporting the extended time observations (ETO) component by collecting polarization lidar and passive radiometric data from high clouds at the University of Utah Facility for Atmospheric Remote Sensing (FARS) during times of Geostationary Operational Environmental Satellite (GOES) and polar-orbiting satellite local imagery. The nature of this unique long-term dataset is reviewed in section 2. Our major goals have been directed toward improving the characterization of cirrus clouds from satellites and developing parameterizations of cirrus radiative properties for application to GCMs. In view of the necessity of obtaining a global understanding of cirrus climatic effects, it is essential that we rely on improved passive, and planned active, remote sensing satellite methods with their global coverage.

In future parts of this series, which will parallel the pioneering group of papers describing the Commonwealth Scientific and Industrial Research Organization ground-based measurements obtained in Australia, we will report on the results of studies using lidar extinction and depolarization, combined infrared radiometric, and radar cirrus cloud measurements at FARS. Specific topics will include characterizing the visible cloud optical thickness, infrared emittance, and cirrus cloud microphysical content derived from lidar depolarization. Finally, note that findings from FARS describing the properties of aircraft condensation trails (contrails), another long-term objective, have recently been reported in Sassen (1997).

2. Cirrus cloud research at FARS

a. Identifying cirrus clouds

The FARS high cloud measurement program, currently in its 13th year, has been conducted under a uniform set of criteria that rely on the visual identification of cloud type. Only a single observer has been responsible for the lidar operations, who received training by the National Weather Service (NWS) as a meteorological technician. Traditionally, a rational scheme for discriminating between the various species of the three main cloud categories (i.e., low, middle, and high clouds) has long been in practice based on visual cloud appearance (Lynch 2001; Sassen 2001). In other words, the perception of cloud height, color, and texture, as depicted in a cloud atlas (e.g., WMO 1987) are relied on. (In our case, the ability of polarization lidar to determine cloud height and phase in real time has helped to refine the process of identifying cloud type.) The three categories are divided into approximate ranges of cloud height (for a given latitude and season), and so by analogy depend on cloud phase. Implicit is the postulate that

the cirrus varieties may contain transient patches of supercooled liquid water clouds (Sassen 2001), but that they are predominantly ice phase clouds. Importantly, in our study no a priori constraints involving cloud height or temperature, or such other factors as lidar or radar signal intensity ranges, are used to define cloud type.

An important factor in distinguishing cloud type is color—the terms translucidus and opacus are applied to layers through which the blue sky color can or cannot be seen by a ground observer, respectively. Thus, estimates of cloud visible optical thickness τ are inherent in the identification of cloud type (Sassen 2001), including the category of subvisual cirrus that had to await the introduction of modern instrumentation. It has been pointed out in Sassen and Krueger (1993) that the capabilities of modern remote sensors should be taken into consideration when it comes to identifying virga, and the same applies to invisible/visible cirrus clouds. When the cloud retains a bluish color from the transmission of skylight, this cirrus is termed *thin.* On the other hand, cirrostratus may gradually thicken from thin to opaque with time, and may become a (similarly ice-dominated) altostratus cloud. These midlevel clouds are operationally distinguished from cirrus by the loss of sharpness or disappearance of the solar disk, and range-limited lidar returns caused by laser pulse attenuation, which occurs when $\tau \gtrsim 3.0$ (Kinne at al. 1992; Sassen and Cho 1992).

b. FARS instrumentation

The Facility for Atmospheric Remote Sensing is a permanent cloud research station located on the eastern edge of the University of Utah campus (40°49′00″N, 111°49′38″E) on the bench of the Wasatch Mountains [1.52 km above mean sea level (MSL)] overlooking Salt Lake City (SLC) in northern Utah. It was established in 1987 with support from the National Science Foundation to house the ruby Cloud Polarization Lidar (CPL), and has steadily grown with the addition of state-of-the-art remote sensors, including visible, infrared, and microwave radiometers, all-sky photographic and video imagery, a 3.2-mm polarimetric Doppler radar, and the dual-wavelength scanning Polarization Diversity (Nd:YAG) Lidar. A description of the entire FARS instrumentation is given in Sassen (1997). Many of these units are mobile and have participated in major cloud research programs.

Because only the two-channel CPL data and extensive field notes are used in this study, we provide in Table 1 the specifications of this long-used ''turnkey'' system. [Components of this lidar can be traced back to one of the earliest systems developed in the mid-1960s at New York University—see Schotland et al. (1971).] Note that the high-power ruby lidar system has a low pulse repetition frequency, and is digitized with a record length of 2048, 8-bit samples at a 7.5-m range resolution. This yields a maximum height of 16.12 km MSL, after accounting for the first 100 pretigger points used to determine the background signal level for each shot. In other words, it generates an amount of data that facilitates the management of an extended remote sensing dataset. On the other hand, the sensitivity of the unit is sufficient to treat each pulse as independent (i.e., no averaging is required for tropospheric targets). Over the years a steady improvement in CPL data acquisition was made by upgrading PC controllers, but a common data archival format has been used throughout.

TABLE 1. Specifications of the Cloud Polarization Lidar at FARS.

Operational	
Wavelength (ruby)	0.694 μm
Peak energy	1.5 J
Maximum PRF	0.1 Hz
Pulse width	25 ns
Polarization	Vertical
Beamwidths: transmitter	0.5 mrad
receiver	1–3 mrad
Receiver diameter	28-cm telescope
Detectors	2, PMTs
Positioning	Manual
Data handling	
Channels	Vertical + horizontal
Sample width (resolution)	7.5 m
Range gates	2048
Digitizer resolution	8 bits
Storage	8-mm tape

c. FARS high cloud data collection philosophy

Since its inception, FARS has been applied to the regular study of high-level clouds in support of basic research and the satellite validation effort of Project FIRE (Schiffer and Rossow 1983; Rossow and Garder 1993). As of December 1999, more than 2750 h of ruby lidar data and nearly 11 000 black-and-white and color fisheye photographs have been collected, largely in accordance with the ephemeris of National Oceanic and Atmospheric Administration (NOAA) polar-orbiting satellite local overpasses. Figure 1 displays the yearly totals of ETO measurement hours since the fall of 1987 when FARS was established, which have since averaged over 200 h per year. More specialized interests in FARS data collection have contributed to the scope of the current dataset, including thin/subvisual studies from 1988 to 1989 and enhanced contrail research from 1993–96. In view of FARS logistical and funding practicalities, a measurement philosophy was adopted early in our program, which deserves discussion in view of its impact on the data record.

The FARS ETO data collection goals emphasized the afternoon and evening hours, corresponding to the local *NOAA-9*, *-10*, *-12*, *-14*, and *-15* platform overpasses, based on a 7-day work schedule. (SLC local time varies from UTC -6 h to -7 h.) Most FARS observations periods are of ~3-h duration. They are designed to en-

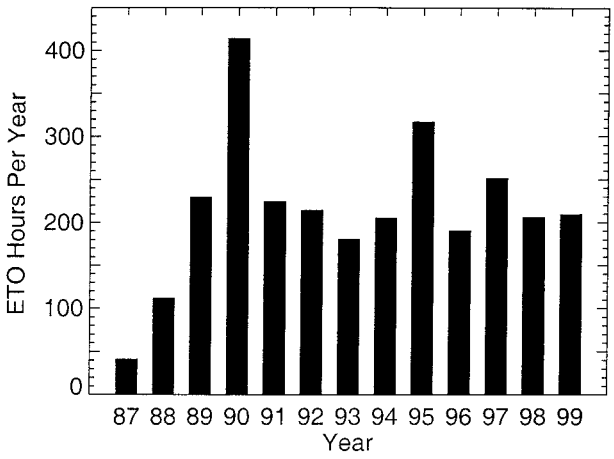

FIG. 1. Record of the number of lidar high cloud extended time observation hours per year since FARS was established in 1987.

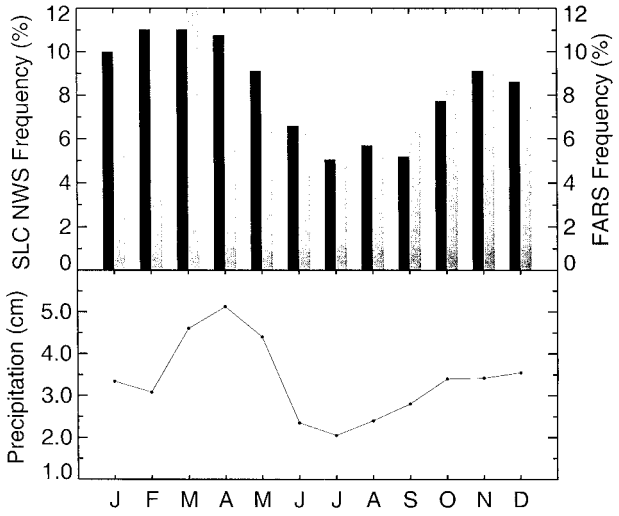

FIG. 2. (top) Comparison of normalized cirrus cloud frequencies based on SLC NWS cloud amount reports (solid bars) and the FARS ETO high cloud data record. (bottom) The monthly average precipitation amounts derived from average SLC NWS data.

compass multiple satellite overpass opportunities, and, importantly, obtain records corresponding to the passage of mesoscale features of advecting cirrus cloud systems. For example, assuming a 25 m s^{-1} mean cirrus level wind speed, a 3-h period corresponds to a 270-km cloud slice: such extended study periods can reveal the passage of entire cirrus cloud systems, or at least identifiable mesoscale components of synoptic features. Depending on local cirrus cloud persistence, however, many shorter periods are present in the dataset. Occasionally an extended ''campaign'' involving multiple periods from a long-lived synoptic cirrus episode lasting a few days or more has been studied. Our resources and scientific priorities allowed for the goal of collecting ~20 h of FARS data per month. Naturally, periods of weeks or more with no observable cirrus (either because of persistent ''severe clear'' or precipitating weather situations) have occurred and restricted data collection at FARS.

Figure 2 demonstrates that this approach has yielded what appears to be an accurate representation of cirrus cloud occurrences at our location. Compared at top are the monthly frequencies of cirrus clouds as determined from the SLC NWS [in terms of the percent of total coverage-weighted amounts, based on data from Hahn et al. (1994)] and from nearby FARS (in percent of total observations). Despite the basic differences in the nature of the datasets, the trends are in good agreement. The largest discrepancies occurring in winter can be attributed to the presence of local low and midlevel orographic clouds that disrupt FARS cirrus observations.

d. The FARS ETO data subset

For the ~10-yr subset of FARS ETO data used here to characterize the macrophysical and synoptic properties of our variety of midlatitude cirrus, we define a cirrus cloud ''data period'' as a 10-min average of cloud layer properties obtained once per hour within ±3 h of the 0000 UTC SLC sounding. The 10-min average data periods correspond to hourly GOES imagery collected just after each hour. Of the ~2200 h of data collected from 1986 to 1996, 1389 data periods are suitable for use here. The basic derived data quantities are the heights of cirrus cloud base and top, which were obtained manually from height versus time plots of lidar backscattering data. These heights were found simply through the use of a rule, effectively to 50-m resolution. Thus the lowest and highest heights showing signals above background/noise levels in each cloud layer identified in the field notes as cirrus were used. In this way, an approximate value suitable for this analysis and similar to that generated by automated algorithms was derived, but only for the visually identified cirrus layers. Then, these heights were converted to values of temporally consistent SLC sounding temperature, pressure, and wind speed/direction.

Of course, during any 10-min period cirrus clouds may not be present or observable due to lower obstructing clouds, as can be appreciated from Table 2. This breakdown by cloud type and cirrus optical thickness category shows that the success rate for studying cirrus was about 90% of the 10-min periods. Moreover, the data are divisible into an average of 2.3-hourly periods per day (corresponding to each ±3 h 0000 interval). An examination of the data monthly breakdown in this subset shows no biases, yielding a histogram very similar to that in Fig. 2.

What is of particular interest in Table 2 is not the division of data periods by cloud type (which is intentionally biased toward cirrus), but rather the cirrus breakdown into the indicated visual zenith characterizations, which has implications for delineating characteristic cirrus cloud τ ranges. According to Sassen and Cho (1992), the following estimations of τ can be

TABLE 2. Breakdown of FARS hourly data collection periods.

	Periods	Frequency
1. Total hourly periods		
(594 independent days)	1389	100%
2. Periods with cirrus present		
Very thin-subvisual ci	217	17%
Thin ci	440	34%
Opaque ci	443	34%
Probable range-limited	91	7%
Definite range-limited	65	5%
Null observations	40	3%
Total periods	1296	
3. Cloud layer observation by type		
Total cirrus	1368	83.5%
As	23	1.5%
Ac	66	4.0%
Ac with virga	40	2.5%
Cu	46	2.5%
Cu with virga	13	1.0%
Low-level crystal layer	75	4.5%
Smoke/aerosol layer	11	0.5%
Total layer heights	1642	

made from their visual appearance: $\tau \lesssim 0.03$ for subvisual, $\tau \lesssim 0.3$ for thin, and $\tau \lesssim 3.0$ for opaque cirrus clouds. The additional definitions in Table 2 for ''probable'' or ''definite'' range-limited cloud-top altitude errors is based on the real-time inspection of the lidar cloud-top signals over an observation period, as routinely mentioned in the field notes for the periods corresponding to GOES imagery. The loss of signals from the upper cloud, which would result in the underestimation of the reported cirrus cloud-top height, is typically a result of the limited dynamic range of the CPL detector package, and so depends on the vertical profile of backscattering through the cloud. In other words, in attempting to avoid off-scale signals, the receiver gain would be reduced, so even a narrow strongly scattering layer could cause a dramatic loss of signals, particularly if the returns from the upper cirrus regions are comparatively weak. Although the two-way laser pulse attenuation through many types of clouds is strong enough to prohibit the detection of cloud top with our lidar, this is generally not as significant a problem as the dynamic range effect in cirrus, because by definition they are optically transmissive (see Sassen 2001).

It is interesting to note that along with the usual cloud categories included in Table 2, the second most commonly detected type is the *crystal layer*, which normally occurs well below cirrus levels. These targets are typically subvisual, but generate strong parallel-polarized backscattering with zenith lidar because they are composed of horizontally oriented planar ice crystals (see Sassen 1991). Since these layers of oriented plates appear to be commonly associated with the glaciation of upwind lenticular altocumulus clouds, it may be that our location in mountainous terrain enhances the frequency of their detection by lidar. However, it should be noted that Vaisala laser ceilometers are being routinely installed worldwide pointing a few degrees off the zenith in order to limit the detection of such subvisual targets (P. K. Piironen 1998, personal communication). The fact that the crystals grow under initially water-saturated conditions, and at relatively warm temperatures, probably explains the tendency for the particles to have the proper shape and size to orient uniformly in space. In addition, the visual difference from cirrus formed in colder orographic clouds is probably a result of the ice nucleation mechanism involved, that is, the rapid homogeneous freezing of haze particles in cirrus versus the heterogeneous freezing of supercooled cloud droplets in altocumulus.

3. Climatological cirrus cloud properties

Here we examine the yearly, seasonal, and monthly means and variabilities in the following cirrus cloud macrophysical and thermodynamical properties; cloud base and top height, temperature, and pressure; height separations of cloud top from the tropopause level; wind direction and speed; cloud layer physical thicknesses; all-sky high-cloud coverages; and cloud visual appearance, from which an estimate of the cloud optical thickness can be obtained. We begin with the mean annual and quarterly statistics of these data quantities.

a. Mean cloud properties

Provided in Table 3 are the seasonal and yearly averages of the cirrus cloud properties characteristic of the FARS location. This sample uses only those cirrus clouds that did not appear to be affected by a loss of cloud-top signals due to the limited dynamic range of the CPL, or range-limiting laser attenuation in the densest cirrus. As mentioned above, the cirrus layer heights were recorded to the nearest 50-m height interval, and the sounding data were chosen to yield representative atmospheric parameters. The tropopause heights used were those identified in the sounding files by the NWS, or when absent (in ~22% of the soundings), using the height of the first temperature inversion above 325-mb pressure. The method for determining the statistics for the cirrus cloud-base and cloud-top heights is based on the *envelope* method, in which either the top and bottom of a single layer or the top of the highest layer and base of the lowest cirrus layer are used. However, also included in Table 3 are the average cirrus layer thicknesses when single and multiple layers are present (89% and 11% of the time, respectively), and the average values of all combined single and multiple layers. These distinctions result from the propensity of some cirrus systems to form and maintain multiple cloud layers (i.e., using the criterion of a >0.5-km gap in lidar signals). However, it is important to recognize that in many instances a single 10-min data period may yield multiple layers that merely represent breaks in a vertically con-

TABLE 3. Seasonal and yearly averages of various cirrus cloud properties derived from the 10-yr FARS dataset.

	Jan–Mar	Apr–Jun	Jul–Sep	Oct–Dec	Annual
Cloud base					
Height (km):	8.40	8.89	9.10	8.89	8.79
Pressure (mb):	353.4	329.9	326.9	332.0	336.3
Temperature (°C):	−38.9	−38.4	−32.6	−39.0	−37.4
Wind direction (°):	288.7	272.5	252.2	281.8	276.3
Wind speed (m s^{-1}):	17.9	16.0	13.9	18.8	16.4
Cloud top					
Height (km):	10.71	11.14	11.12	11.15	11.02
Pressure (mb):	248.2	235.1	243.5	233.9	240.2
Temperature (°C):	−55.8	−55.3	−47.6	−55.9	−53.9
Wind direction (°):	285.0	270.8	252.9	284.9	275.7
Wind speed (m s^{-1}):	23.9	19.8	17.0	21.3	20.2
Separation from tropopause (km)					
Average SLC soundings	0.14	0.86	3.06	0.42	1.17
Cirrus day soundings	0.64	1.09	3.09	1.06	1.49
Cloud thickness (km)					
Layer envelope	2.31	2.25	2.02	2.26	2.23
Multiple layer	1.32	1.13	1.17	1.38	1.24
All layers	1.93	1.72	1.60	1.91	1.81
Sky coverage (%)					
Overcast	75.7	63.9	40.5	69.2	64.9
Broken	19.4	30.8	49.4	22.6	29.0
Scattered	4.9	5.0	10.1	4.8	6.0
Visual appearance (%)					
Opaque	42.7	54.3	59.8	41.6	48.2
Thin	39.9	28.9	33.8	38.0	35.4
Threshold/subvisible	17.2	17.7	6.4	20.5	16.4

tinuous cloud, which result from the effects of vertical wind shear on fall streaks.

The final two categories provide supplemental information on the prevailing cirrus all-sky coverage and the visual appearance (color) of the cirrus in the zenith at the time of each observation. For sky coverage, overcast is >90%, broken 50%–90%, and scattered 5%–50% cloud coverage. This differs slightly from the NWS approach, but was adopted here because cirrus overcasts frequently contain barely (i.e., *threshold*) visible or subvisual parts, and even minor amounts of clouds could fill radiometer pixels and be sensed by satellites in the vicinity of FARS.

Although the data in Table 3 represent the most comprehensive examination of cirrus properties assembled to date from a particular location using remote sensors, the mean yearly or seasonal properties do not provide the complete picture regarding cirrus. Rather, it is important to understand their inherent variability on shorter timescales, as is analyzed below.

b. Monthly variability of cirrus properties

The unique FARS high cloud dataset is of sufficient size to permit the assessment of the variability in cirrus properties on a monthly timescale. We begin this assessment with Fig. 3, which summarizes the monthly mean values for cirrus cloud-base (dashed) and -top (solid) heights, temperatures, pressures, and wind directions and speeds. Figure 4 compares the mean monthly values for cirrus cloud-top heights with the SLC sounding tropopause heights derived both from a recent 10-yr average, and using the same sample of cirrus days contained in the ETO dataset. Note that SLC tropopause heights shown as solid squares are, except in summer, significantly higher than the long-term average, showing that the cirrus days are accompanied by elevated tropopauses. As above, we confine this analysis to the envelope data sample, and ignore the relatively small portion of range-limited cloud-top height measurements (~14% of the total cirrus sample, see Table 2). Note, however, that including these data has only a minor impact on the average cirrus characteristics (Campbell 1997).

It is apparent from Fig. 3 that the cirrus cloud properties follow seasonal cycles, which is particularly clear in the atypical summer season temperatures, and wind directions and speeds. Although cirrus cloud-top heights do not show a strong seasonal trend, and peak in the fall, Fig. 4 demonstrates that with respect to their separation from the tropopause, summer cirrus cloud heights are distinct. The variabilities inherent in these monthly mean cirrus cloud-top and -base heights and temperatures, and height separations from the tropopause are revealed in Figs. 5, 6, and 7, respectively. Here, the effects of seasonallity are again in evidence.

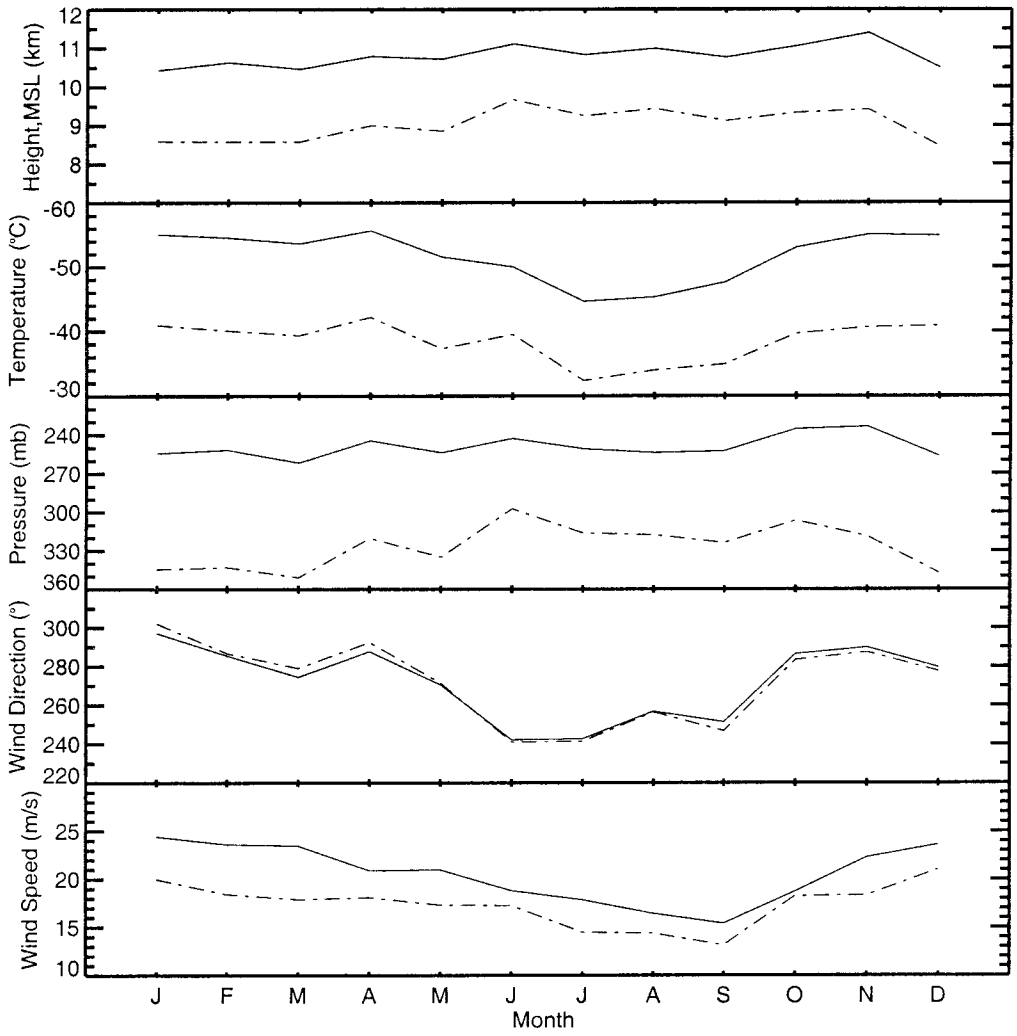

FIG. 3. Comparison of monthly averaged cirrus cloud-top (solid) and cloud-base (dashed) heights, temperatures, pressures, and wind speeds and directions, derived from the 10-yr FARS dataset.

Finally, shown in Fig. 8 is a bargraph showing the monthly changes in mean cirrus cloud layer thicknesses, for cases having single and multiple layers, and the average of all cases. To understand their variability, Fig. 9 portrays the probability density functions in percent of the total seasonal and yearly cloud layer thicknesses for the combined single and multiple layers. An analysis of these seasonal variations, to understand why they occur, is provided in section 4.

c. Cirrus wind roses

Depicted in Fig. 10 is a collection of yearly plus seasonal wind directional frequencies and average speeds plotted as wind roses, from which the variability around the mean values given in Table 3 can be appreciated. Although these data correspond to the cirrus cloud-top heights, the results using the cloud-base winds are quite similar because of the lack of significant average directional wind shear (Fig. 3). The wind roses were constructed by totaling all cloud-top wind observations within 15° radial bins, computing their relative occurrence frequencies, and averaging the wind speeds within each bin. This totaled 1166 data periods.

The cumulative annual wind rose in Fig. 10a illustrates that while the vector average cirrus radiosonde winds in Table 3 were nearly due westerly, higher directional frequencies are present with southwesterly flow and the highest speeds are out of the northwest, which therefore influenced the vector average. Although infrequent, southeasterly winds are also present during some seasons, which is indicative of cutoff low pressure systems that occasionally situate themselves south of SLC.

4. Synoptic conditions and FARS cirrus properties

Here we provide a brief characterization of the weather of the Great Basin in general, and the SLC region in

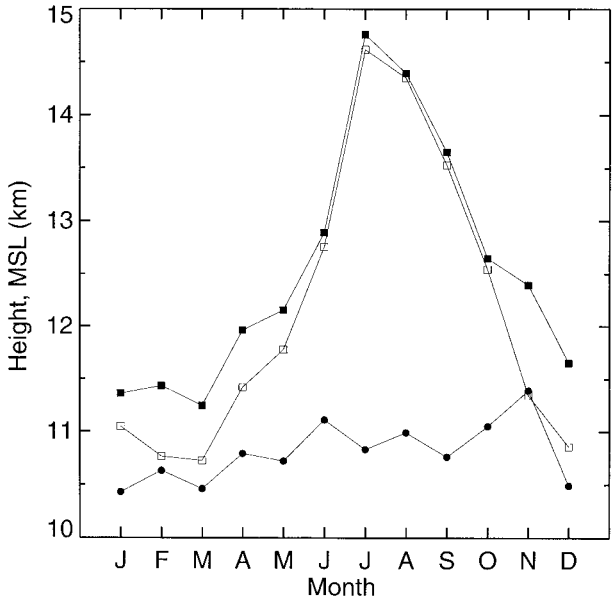

FIG. 4. Monthly averaged cirrus cloud-top heights (circles) contrasted with SLC tropopause heights derived from a 10-yr sounding average and the average of the cirrus ETO sample, open and solid square symbols, respectively.

particular, because it is clear that synoptic weather patterns and the occurrence of cirrus are intrinsically related (Stone 1957; Starr and Wylie 1990). The above findings are analyzed in this context to better comprehend the seasonal properties of the cirrus clouds observed at FARS. We stress that to understand the relevance of the FARS cirrus cloud data record it is necessary to know how the observed cirrus were generated, and how typical these generating mechanisms are of the midlatitudes.

a. Synoptic flow patterns associated with cirrus

A climatological examination of the upper-level flow regimes associated with the generation and transport of cirrus over northern Utah is provided here to statistically relate the occurrence of cirrus in our sample to the upper-level patterns common to the area. Specifically, we examine the monthly frequencies of five synoptic flow regimes corresponding to 508 days when cirrus were studied at FARS. Each day was examined to identify which of the following patterns was present and responsible for cirrus clouds over SLC: (i) a ridge with strong amplitude, (ii) a flat ridge, (iii) zonal jet stream flow, (iv) split flow with a low pressure center in the lower subtropical branch or cut off from the main circulation, and (v) a trough where the midlatitude jet was in phase with the subtropical jet.

These statistics rely on an inspection of 1200 UTC 500-mb synoptic maps (~12 h before the cirrus periods) to identify each days dominant flow pattern. For nonridge cases, the pattern type and 500-mb height at SLC was extrapolated and recorded. For ridge cases, the latitudinal ridge axis position and 500-mb height along 40°N was instead noted, and it was determined whether or not 120 m of depth on either side of its axis along 40°N existed. This standard determined the extent of amplitude to the system, producing the division of ridge cases into two groups (i and ii). Figure 11 displays typical examples of each of the five cases, showing the 1200 UTC 500-mb map superimposed over the corresponding infrared satellite imagery.

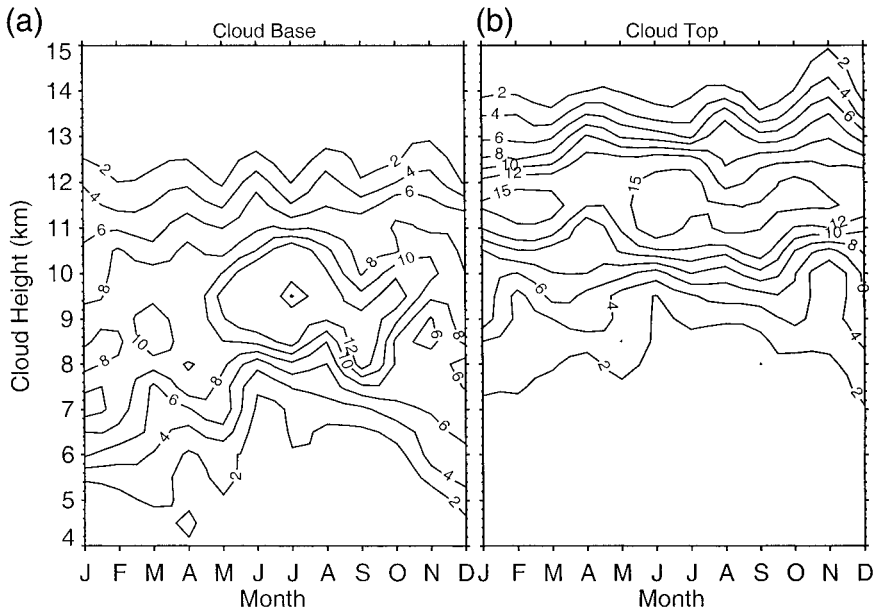

FIG. 5. Monthly frequencies of cirrus (a) cloud-base and (b) cloud-top heights MSL, in percent using 0.5-km intervals.

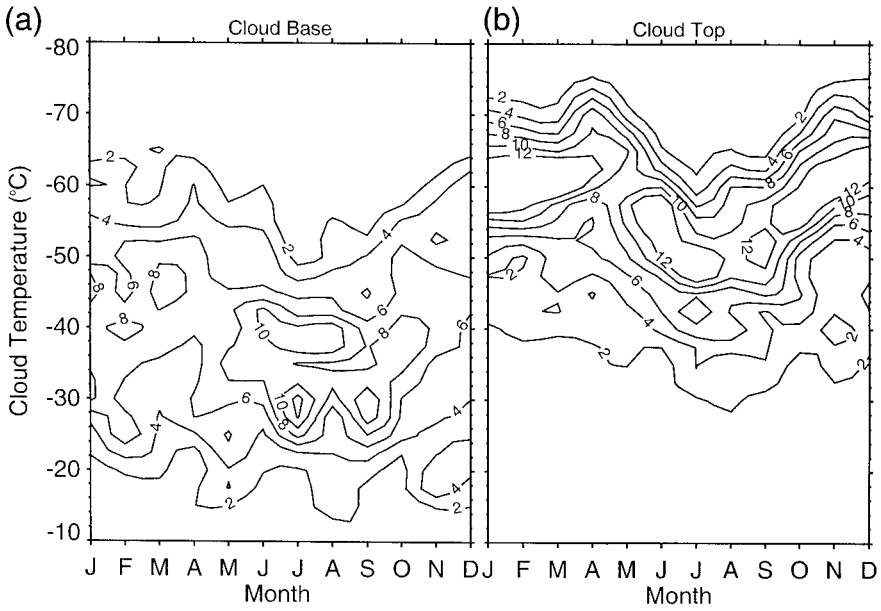

FIG. 6. Monthly frequencies of cirrus (a) cloud-base and (b) cloud-top temperatures, in percent using 2.5°C intervals.

Table 4 provides a breakdown of the results for each of the five synoptic types, including their frequencies, average 500-mb heights, and corresponding average cirrus cloud-top heights and wind data. In addition, ridge cases have been broken into 10° latitudinal bins. Ridges with significant amplitude are the most commonly observed synoptic feature, while zonal flow and split flow cases have lower but significant rates of occurrence. Not surprisingly, the lowest observed cloud-top heights coincide with relatively cold trough cases, while the highest coincide with flat ridge cases. Table 5 breaks the pattern frequencies into monthly totals. Ridge cases with strong amplitude are prevalent throughout the year, while flat ridges occur mostly between June and September. Zonal flow and split flow are most common during the transitional seasonal months, and trough cases are seen mostly during winter months.

Over 25% of these cirrus cases coincide with an amplified ridge with its axis situated to the west of SLC, where conditions marked by large-scale subsidence and stability are to be expected. Mostly observed in winter

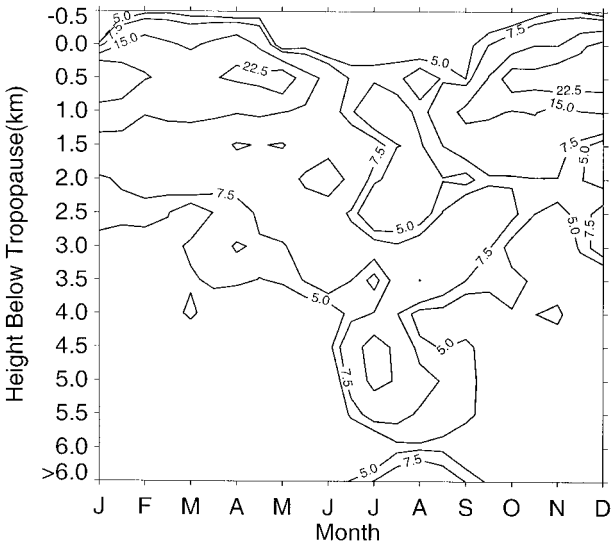

FIG. 7. Monthly frequencies of height separation between cirrus cloud-top and the corresponding tropopause heights, in percent using 0.5-km intervals.

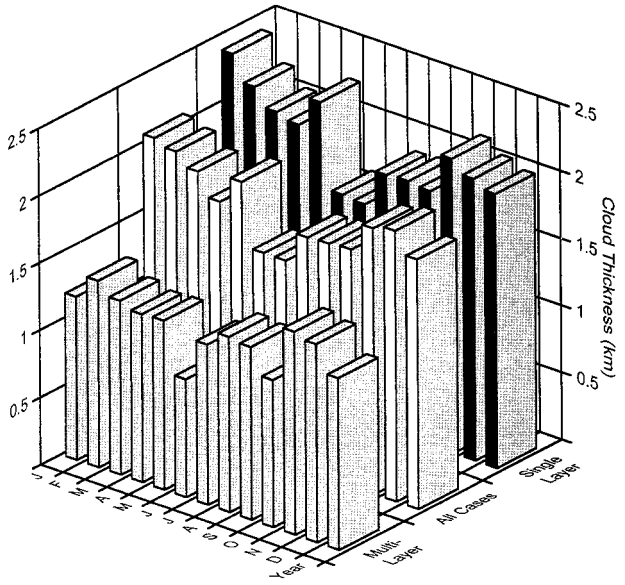

FIG. 8. Bar graph of monthly averages of cirrus cloud physical thicknesses for multilayer, single layer, and the combined dataset.

TABLE 4. Cumulative synoptic flow pattern statistics for cirrus days.

	Frequency	500-mb height	Height MSL (km)	Direction (°)	Speed (m s^{-1})
Zonal flow	0.23	5678*	10.8	275	25.2
Split flow/cutoff	0.24	5678*	10.3	248	18.9
Trough	0.06	5579*	9.92	245	22.9
Ridge (total)	0.37	5793**	10.9	288	19.4
≥20°W	0.05	5810	9.95	287	23.6
19°–10°W	0.11	5792	10.8	310	23.0
10°–0°W	0.12	5758	11.3	296	21.2
0°W–10°E	0.07	5827	11.0	248	17.2
≥10°E	0.02	5848	11.8	225	24.4
Flat ridge (total)	0.10	5865**	10.9	263	17.3
≥20°W	0.00	—	—	—	—
19°–10°W	0.01	5857	11.5	287	25.3
10°–0°W	0.02	5873	10.8	272	14.0
0°W–10°E	0.06	5864	10.7	254	18.1
≥10°E	0.01	5860	11.7	238	16.7

* 500-mb height level for zonal, split flow/cutoff, and trough situations is that at SLC.

** 500-mb height for both ridge cases is that at ridge axis along 40°N.

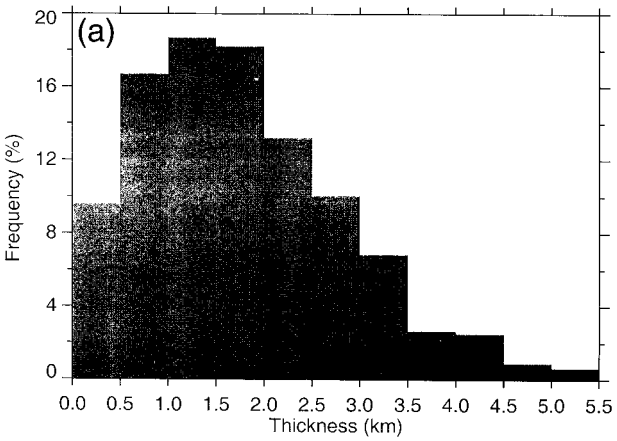

FIG. 9. Frequency of occurrence of 0.5-km intervals in cirrus layer thicknesses (including both single and multiple layers) for (a) annual and (b)–(e) seasonal averages (facing page).

months, the ridge axis is often >10° west of SLC (such as in the example in Fig. 11a).

b. Weather and cirrus over the eastern Great Basin

In general, two basic synoptic upper-level features influence weather over the western United States: a subtropical high pressure complex centered over the eastern Pacific Ocean, termed the Pacific Ridge, and the midlatitude jet stream pattern found near 300 mb (Davis and Walker 1992). Since SLC lies approximately 1000 km east of the Pacific coast near 40°N, its position relative to the axis of the Pacific Ridge is seasonally dependent. This feature is displaced southwestward during the winter, and as meridional temperature gradients increase, strong jet stream systems allow cold air to be advected southward. During the summer, its mean position shifts inland amidst weak westerlies, and monsoonal conditions are prevalent. Topography also influences the weather of the Great Basin. Numerous mountain ranges lie between SLC and the primary moisture source of the Pacific Ocean, which tend to be barriers to the low-level flow of moisture and precipitation. FARS is surrounded by the Wasatch Mountains to the east (with peaks up to ~3.5 km), and the Oquirrh Mountains to the west (with ~3.0 km peaks), such that the effects of local terrain can be important in terms of local cloud and precipitation formation. The SLC NWS office, which lies ~12 km to the west and 230 m below FARS, receives about 40 cm of precipitation a year (Fig. 2).

During summer months, the position of the Pacific Ridge is well onshore, and midlatitude jet stream flow is weakened by mild meridional temperature gradients. Typically, storms stay well to the north of the region. An analysis of mean SLC wind profiles indicates that the Pacific Ridge axis is situated nearly overhead of SLC between April and June, and to the east from July to September (Campbell 1997). Although unstable impulses do propagate through the weak steering currents, summer precipitation is heavily dependent on the onset of monsoonal conditions, which generally become favorable beginning in late June. Southwesterly flow aloft is augmented near the surface by circulation around a surface low pressure system in southwestern Arizona induced by strong solar heating (the so-called thermal low). Both advect subtropical moisture from the Pacific Ocean, Gulf of California, and Gulf of Mexico producing unstable conditions along the western side of the ridge axis (Adams and Comrie 1997). Surface solar heating induces afternoon thunderstorms, particularly over mountainous terrain, thus providing a source of regional mid and high clouds.

Locally observed cirrus typically result from thunderstorm anvil blow-off advected upstream from generally more active source regions to the south. Although anvils from cumulonimbus induced by the local terrain are represented in the dataset, SLC lies on the northern edge of the monsoonal circulation where moisture is less abundant and local thunderstorms are generally less frequent. Low-level instabilities are subsequently less imposing, such that local thunderstorm tops regularly

TABLE 5. Monthly frequencies in percent of the five common synoptic patterns responsible for cirrus over the eastern Great Basin.

	Jan	Feb	Mar	Apr	May	Jun	Jul	Aug	Sep	Oct	Nov	Dec
Ridge	46	47	32	50	26	33	13	46	37	37	36	28
Flat ridge	0	0	2	0	2	18	63	37	12	0	5	0
Zonal	22	16	29	29	31	13	7	5	12	37	45	33
Split flow	29	33	35	10	36	21	17	10	35	20	14	26
Trough	2	4	3	10	5	15	0	2	5	2	0	14

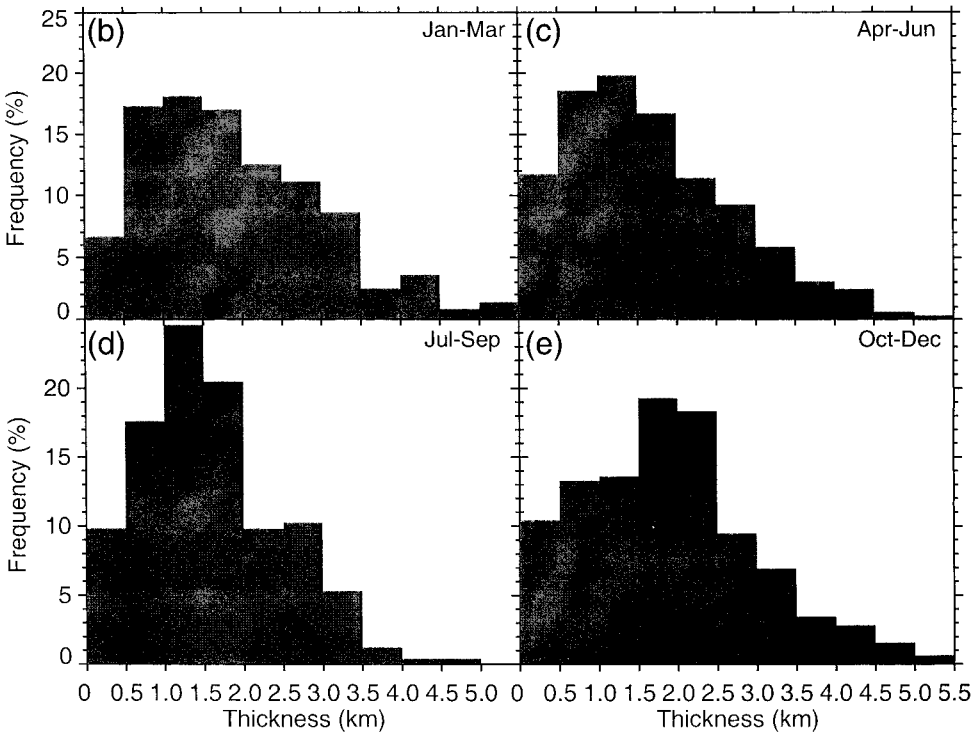

FIG. 9. (*Continued*)

fail to approach the tropopause level. With mean tropopause heights of >13.5 km, Fig. 4 shows that the mean cirrus cloud tops are situated up to 4 km below the tropopause. Not unexpectedly, both the average summer precipitation and cirrus frequencies are the lowest of the year (Fig. 2). Mean cloud thicknesses (Figs. 8 and 9) are unusually thin, and most cases are found in weak southwesterly flow (Figs. 3 and 10). Eighty percent of these cases are associated with ridging conditions (Table 5).

Monsoonal conditions relax by October. In fall, the midlatitude westerlies pick up and cases of zonal and northwesterly flow become more common. The mean Pacific Ridge axis position shifts west of SLC during October, and the reemerging subtropical jet increases the frequency of split jet stream cirrus cases. The fall season wind rose (Fig. 10d) displays variable directional frequencies, with most occurring in northwesterly midlatitude jet stream flow along the rear side of the Pacific Ridge axis. Increased wind speeds reflect the strengthening of the westerlies. Interestingly, the highest average cloud-top heights are observed in November (Fig. 3). This is the result of tropical moisture and cirrus advection in mostly zonal flow. Warm fronts are sometimes noted to the north of SLC as these conditions develop. Mean tropopause heights are still relatively high (Fig. 4), and cirrus increasing approach the altitude of this stable layer (Fig. 7).

Winter conditions at SLC from December through February are typically relatively dry (Fig. 2) as the strength of the Pacific Ridge reaches a maximum, and upper-level moisture a minimum. The prevailing winds shift to northerly (Fig. 10b), which limits moisture advection from the Pacific Ocean and allows cold, dry continental air to dominate the area. A 500-mb synoptic climatology for the western United States (Paegle and Kierulff 1974) shows a broad, flat ridge centered off the west coast as the predominant flow pattern beginning in December. Cases of zonal flow decrease abruptly, as four of the five synoptic patterns show nearly even distributions (Table 5). By January most cirrus are associated with large-scale ridging in north to northwesterly flow, though zonal and split flow cases are also common. Mean tropopause and cirrus cloud heights decline (Fig. 4). Both wind speeds and cloud depths are at or near annual maxima, yet the greatest amount of optically thin cirrus are observed in winter (Table 3). Given the usual proximity and strength of the Pacific Ridge, winter cirrus over SLC are often in a decaying state, advected by rapid jet stream flow well downstream from their generating sources. In other words, the cirrus persist along the advancing side of upper-tropospheric high-pressure ridges (Table 4), where cirrus production is not normally anticipated. Their ability to overcome the broad upper-level synoptic stability and ambient subsidence to spread so far inland is surprising.

The spring transitional period begins in March and extends through June as meridional temperature gradi-

ents increase and the midlatitude jet stream activity increases. The organized weather systems that advance through the westerlies are responsible for both the highest cirrus frequencies and the highest seasonal precipitation amounts at SLC (Fig. 2). The mean position of the Pacific Ridge axis is displaced southeastward toward its deamplified summer position by July, and cases associated with ridging decrease as zonal and split flow increase. Few subtropical jet cases occur. Average cloud boundary and tropopause heights begin a gradual increase (Figs. 3, 4). Ridge-associated northwesterly winds decline, particularly in June when cases of southwesterly flow indicative of the shifting ridge axis become significant. This feature correlates with the onset of cases associated with flat ridging (Table 5). The mean heights of the SLC tropopause and the cirrus cloud tops separate abruptly in May (Fig. 4). During colder months, the correlation between the two indicate a strong association with jet stream flow. As summer monsoonal conditions approach, and the magnitude of the westerlies gradually weakens, cirrus are more frequently associated with weak impulses where the clouds are in a decaying stage.

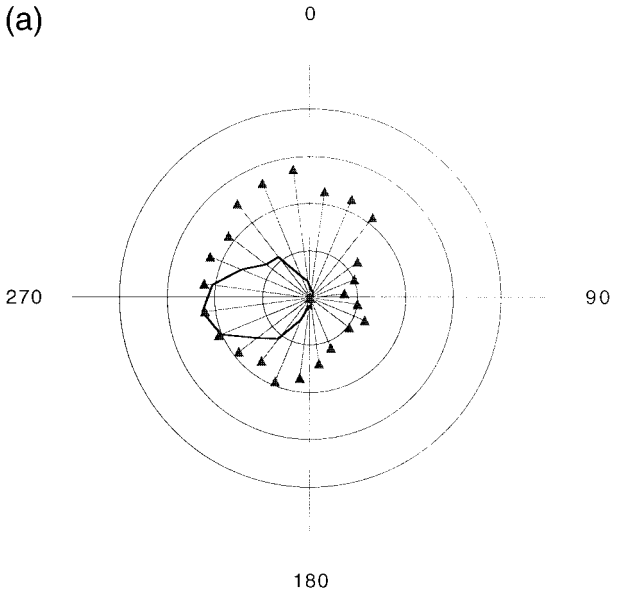

FIG. 10. (a) Annual and (b)–(e) seasonal (Jan–Mar left through Oct–Dec right, facing page) cirrus cloud-top altitude wind roses, showing wind directions in 15° intervals (heavy lines, where each ring represent 7% of the sample) and the corresponding average wind speeds (radiating lines, where each ring is 10 m s^{-}).

5. Conclusions

In this first part of a series of papers describing the climatological properties of the midlatitude cirrus clouds intensively studied from FARS for over a decade, we have reported their essential macrophysical and synoptic characteristics. In each of the 508 independent case studies treated here, the cirrus clouds were identified through the traditional, phenomenological classifications based on visual inspection from the ground. Although cirrus overlying lower clouds were generally not studied because of the limitations of lidar probing, it is doubtful that the properties of cirrus in multilayered cloud systems would differ significantly from those studied here. The cirrus thermodynamic properties, based on 50-m height resolution lidar cloud boundary data, were taken from nearly coincident NWS sounding profiles to ensure their compatibility. Clearly, the accumulation of similarly comprehensive information from a number of surface sites would be highly useful for better understanding the radiative impact of cirrus on a more global scale.

In terms of basic cirrus cloud research, the findings reported here provide for an effective definition of midlatitude cirrus with regard to the fundamental formation mechanism. Since only ~2% of the cirrus have cloud-top temperatures warmer than −40°C, and most of these have likely resulted from the sampling of sheared precipitation streaks generated aloft, it is indicated that supercooled liquid cloud layers cannot contribute significantly to what are visually identified as cirrus clouds. [The few exceptions to this rule are discussed in Sassen (2001).] Since at this temperature homogeneous freezing would prohibit the existence of highly supercooled water (Pruppacher and Klett 1997), cirrus cloud formation must predominantly be caused by the freezing of submicron haze particles. In view of this nucleation scenario and earlier in situ measurements (Sassen and Dodd 1988; Heymsfield and Miloshevich 1995), we recommend that in studies lacking visual cloud observations, a minimum cloud-top temperature of −37°C be employed to ''identify'' cirrus. Our dataset also shows that our cirrus cloud-top heights typically approach the tropopause, except during the summer season under conditions of weak monsoonal thunderstorms. Although the cirrus properties vary significantly in response to seasonally prevalent weather patterns, 10-yr average values for our local cirrus cloud-base/top properties are 8.79/11.2-km height, 336/240-mb pressure, −34.4/−53.9°C temperature, 16.4/20.2 m s^{-1} wind speed, and 276.3/275.7° wind direction. The average cirrus layer physical thickness for both single and multiple cloud layers is 1.81 km.

Because cirrus clouds are a product of weather processes that inject water vapor into the dry upper troposphere (only to be subsequently removed through cirrus particle sedimentation), it is expected that local cirrus cloud properties will depend significantly on geographic location and the prevailing upper-level weather patterns. In view of the fact that weather is a strong function of latitude (i.e., solar heating and its redistribution) and longitude (a consequence of circulations to seasonally fall into synchronization with major topographical features), we caution that our findings are very likely to be site specific to the eastern Great Basin of the western United States. It has already been pointed

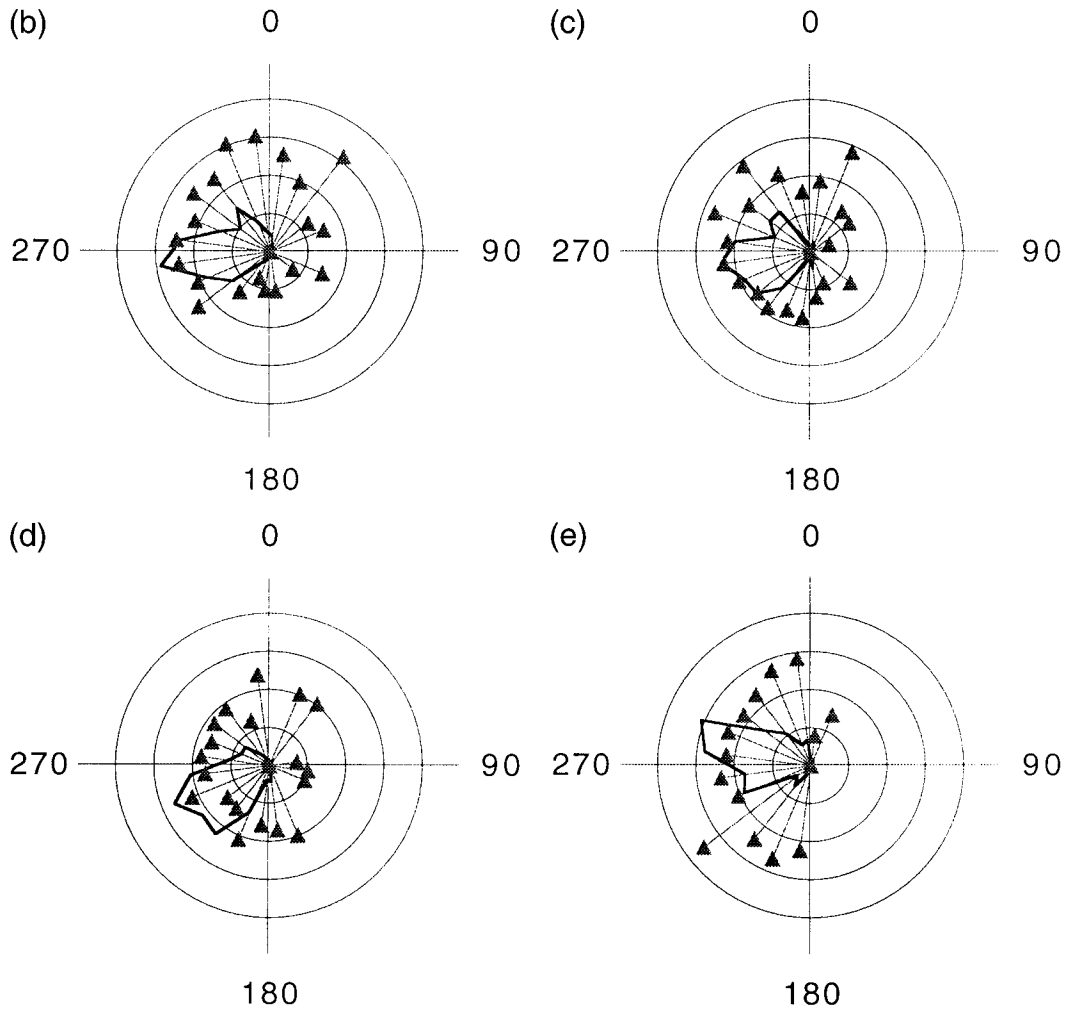

FIG. 10. (*Continued*)

out using a small subset of our data in Sassen and Cho (1992) that significant differences in cirrus properties appear to exist from location to location. Thus we have thought it important to describe the synoptic generation of our local cirrus. We conclude that the genesis of cirrus clouds observed over FARS falls into two basic categories, with transitional stages, that depend on the season.

During the summer season, the main source of cirrus is the residual effects of monsoonal cumulonimbus clouds—anvils derived from both local (orographic) and more distant sources in the Southwest. In contrast, during the winter and transitional periods, the local cirrus are primarily the result of clouds advected by midlatitude jet streams propagating eastward from synoptic-cloud-generating regions over the Pacific Ocean. The local orographic generation of cirrus wave clouds is not uncommon, though, because of our mountainous terrain. Polar cold frontal outbreaks are rare, but when they occur they can generate the lowest cirrus clouds. Although subtropical jet streams infrequently penetrate into the northern Great Basin, subtropical and tropical (hurricane-induced) cirrus can be entrained into large amplitude upper-air wave patterns, particularly during spring and fall as maritime-Pacific storms are moving onshore. With regard to cirrus generation from surface features, strong cyclogenesis is infrequently observed as regional topography effectively inhibits the necessary low-level support. Although warm fronts are uncommon, they are associated with the highest cirrus clouds observed at FARS. It is unlikely that any other location on Earth encounters this particular blend of synoptic and mesoscale cirrus formation mechanisms.

In this context, we find it significant that over 25% of our cirrus cases are associated with a ridge situated with its axis often well to the west of SLC (Table 5). This is a surprising result: traditional thinking would not associate cirrus with stable conditions marked by large-scale subsidence. Yet much of our cirrus are found where clouds are essentially decaying. Thus, cirrus cloud lifetimes appear surprisingly resilient in view of

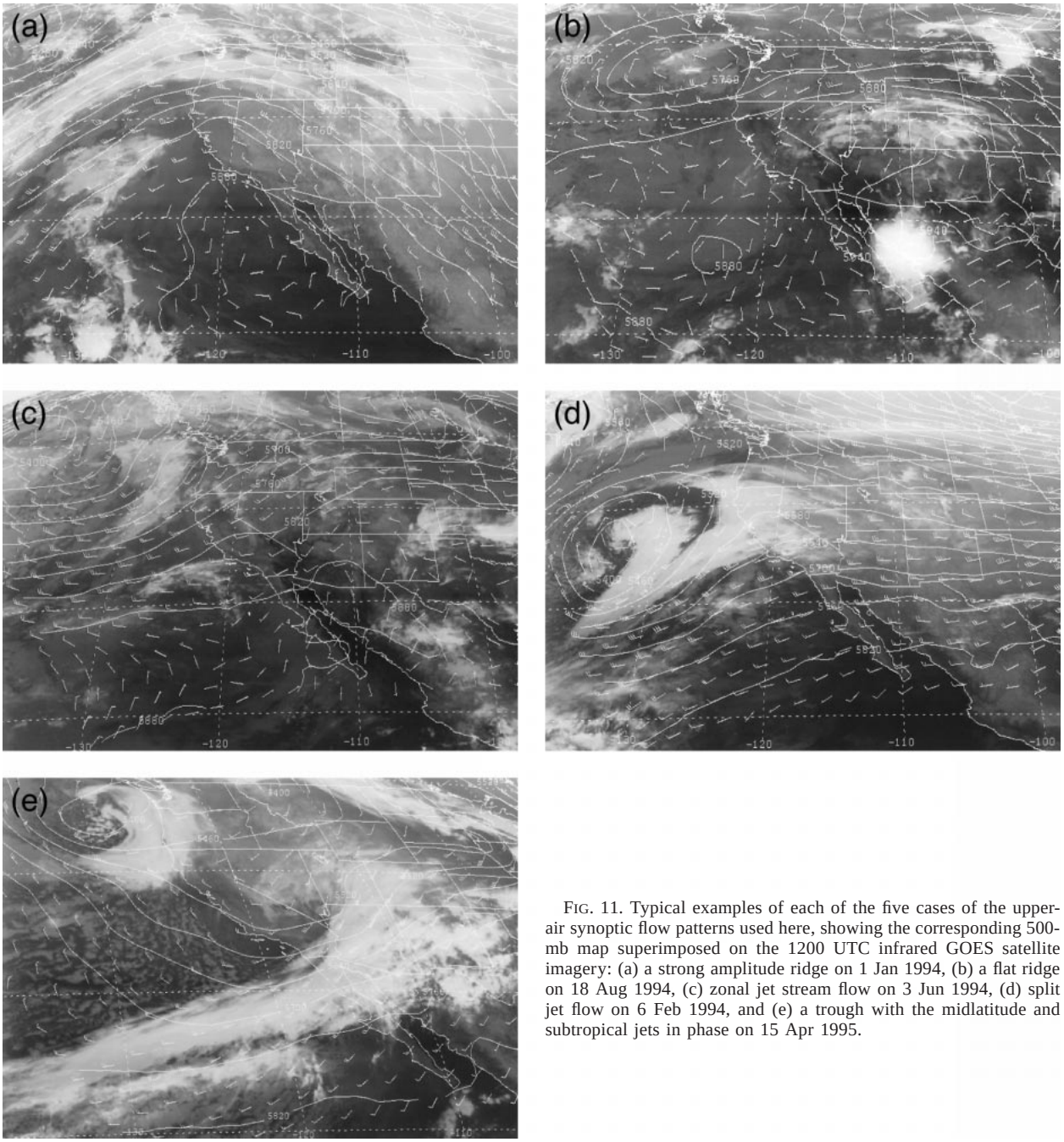

FIG. 11. Typical examples of each of the five cases of the upper-air synoptic flow patterns used here, showing the corresponding 500-mb map superimposed on the 1200 UTC infrared GOES satellite imagery: (a) a strong amplitude ridge on 1 Jan 1994, (b) a flat ridge on 18 Aug 1994, (c) zonal jet stream flow on 3 Jun 1994, (d) split jet flow on 6 Feb 1994, and (e) a trough with the midlatitude and subtropical jets in phase on 15 Apr 1995.

the unfavorable growth conditions. While mesoscale impulses and cloud-scale convection likely subsidize local dynamics, aiding in cloud maintenance under these conditions, this finding raises basic questions regarding the relationship between cirrus cloud lifetime and ambient conditions. Both this experimental finding and model studies (Khvorostyanov and Sassen 1998) indicate a fundamental *slowness* in the cirrus ice particle growth and evaporation processes.

Considering the current dearth of extended time cloud datasets, a number of research applications can be anticipated.[1] In addition to enhancing our basic knowledge of cirrus clouds as discussed above, the FARS dataset offers opportunities for the testing of GCM cirrus cloud height, temperature, or pressure predictions in our geo-

[1] To facilitate the dissemination of the dataset in digital form, it is available through the NASA Goddard Global Change Master Directory, http://gcmd.gsfc.nasa.gov.

graphical location. In addition to cloud microphysics, these properties have a significant impact on radiative transfer through the atmosphere. Thus, correctly predicting cirrus cloud heights is an important step in improving weather and climate predictions, although the model layer height resolutions for the upper troposphere typically used in GCMs exceed the majority of cirrus cloud layer thicknesses shown in Figs. 8 and 9, and cirrus layers are often spatially inhomogeneous. Thus, model parameterizations that account for such subgrid-scale phenomena must be developed and applied.

Finally, the dataset should be applied to its *intended* purpose in supporting Project FIRE—testing and improving the methods for sensing cirrus clouds using multispectral radiance observations from satellites. As recognized in the design of Project FIRE, the study of cirrus clouds using orbiting radiometers has always been difficult for a number of reasons (Minnis 1998), which are related to their quintessential optical nature: cirrus are optically thin in the visible and gray body emitters in the infrared. A climatological intercomparison of SLC-area cirrus cloud properties using passive satellite and active FARS data will have to overcome some considerable difficulties, however.

The first problem is caused by cirrus that are too optically thin to be reliably detected by current satellites. It can be inferred from the cirrus cloud visual appearance information in Table 3 that about one-half of our sample was ''thin'' cirrus, with $\tau \approx 0.3$ or less. It must be known what percentage of these cirrus can be detected with available satellite methods. The second problem deals with the manner in which those *cold* and *high* clouds that are detected are correctly classified as cirrus from the top of the atmosphere. Acknowledging that surface weather observers have traditionally defined cirrus clouds, it is clear that cirrus can be misidentified from satellites unless their optical depths are limited to those that are reasonable for cirrus, say $\tau \approx 3$–5. In other words, the tops of precipitating clouds, even if cirruslike, must not be categorized as cirrus. The alternative would be to ignore the traditional conceptualization of cirrus and make ground- and satellite-based climatologies irreconcilable.

Nonetheless, it is imperative that satellite cirrus cloud measurement capabilities be improved so that it is possible to obtain more accurate global views of their distribution and properties. Along with ground-based studies such as described here, planned Earth-orbiting lidars and radars offer considerable promise to supplement and improve the passive methods, which are themselves evolving as part of NASA's Earth Observing System program.

Acknowledgments. Recent FARS cirrus cloud research has been funded by NSF Grant ATM-9528287 and NASA Grant NAG-2-1106. We thank Z. Wang, J. M. Barnett, and B. McDonald for their contributions. Author KS acknowledges his youthful training by the (then) Weather Bureau in facilitating a career of cloud research.

REFERENCES

Adams, K., and A. C. Comrie, 1997: The North American monsoon. *Bull. Amer. Meteor. Soc.,* **78,** 2197–2213.

Campbell, J. R., 1997: A midlatitude cirrus climatology from the ten-year facility for atmospheric remote sensing high cloud dataset. M.S. thesis, Department of Meteorology, University of Utah, 112 pp.

Cox, S. K., D. S. McDougal, D. A. Randall, and R. A. Schiffer, 1987: FIRE—The First ISCCP Regional Experiment. *Bull. Amer. Meteor. Soc.,* **68,** 114–118.

Davis, R. E., and D. R. Walker, 1992: An upper-air synoptic climatology of the western United States. *J. Climate,* **5,** 1449–1467.

Hahn, C. J., S. G. Warren, and J. London, 1994: Edited synoptic cloud reports from ships and land stations over the globe, 1982–1991. Internal documentation, Data Support Section, NCAR.

Heymsfield, A. J., and L. M. Miloshevich, 1995: Relative humidity and temperature influences on cirrus formation and evolution: Observations from wave clouds and FIRE-II. *J. Atmos. Sci.,* **52,** 4302–4326.

Imasu, R., and Y. Iwaska, 1991: Characteristics of cirrus clouds observed by laser radar (lidar) during the spring of 1987 and the winter of 1987/88. *J. Meteor. Soc. Japan,* **69,** 401–411.

Khvorostyanov, V. I., and K. Sassen, 1998: Cirrus cloud simulation using explicit microphysics and radiation. Part II: Microphysics, vapor and mass budgets, and optical and radiative properties. *J. Atmos. Sci.,* **55,** 1822–1845.

Kinne, S., T. P. Ackerman, A. J. Heymsfield, F. P. J. Valero, K. Sassen, and J. D. Spinhirne, 1992: Cirrus microphysics and radiative transfer: Cloud field study on 28 October 1986. *Mon. Wea. Rev.,* **120,** 661–684.

Liou, K.-N., 1986: The influence of cirrus on weather and climate processes: A global perspective. *Mon. Wea. Rev.,* **114,** 1167–1199.

Lynch, D., 2001: Cirrus: History and definition. *Cirrus,* D. Lynch et al., Eds., Oxford University Press, in press.

Minnis, P., 1998: Retrieval of cloud properties from satellite data for weather and climate forecasting. *Proc. WMO Workshop on Cloud Measurements for the Forecast of Weather and Climate,* Mexico City, Mexico, WMO, 60–72.

Paegle, J. N., and L. P. Kierulff, 1974: Synoptic climatology of 500-mb winter flow types. *J. Appl. Meteor.,* **13,** 205–212.

Platt, C. M. R., J. C. Scott, and A. C. Dilley, 1987: Remote sounding of high clouds. Part VI: Optical properties of midlatitude and tropical cirrus. *J. Atmos. Sci.,* **44,** 729–747.

——, S. A. Young, P. J. Manson, G. R. Patterson, S. C. Marsden, R. T. Austin, and J. H. Churnside, 1998: The optical properties of equatorial cirrus from observations in the ARM Pilot Radiation Observation Experiment. *J. Atmos. Sci.,* **55,** 1977–1996.

Pruppacher, H. R., and J. D. Klett, 1997: *Microphysics of Clouds and Precipitation.* 2d ed. Kluwer, 954 pp.

Raschke, E. J., J. Schmetz, J. Heintenberg, R. Kandel, and R. W. Saunders, 1990: The International Cirrus Experiment (ICE)—A joint European effort. *ESA J.,* **14,** 193–199.

Rossow, W. B., and L. C. Garder, 1993: Cloud detection using satellite measurements of infrared and visible radiances for ISCCP. *J. Climate,* **6,** 2370–2393.

Sassen, K., 1991: The polarization lidar technique for cloud research: A review and current assessment. *Bull. Amer. Meteor. Soc.,* **72,** 1848–1866.

——, 1997: Contrail-cirrus and their potential for regional climate change. *Bull. Amer. Meteor. Soc.,* **78,** 1885–1904.

——, 2001: Cirrus clouds: A modern perspective. *Cirrus,* D. Lynch et al., Eds., Oxford University Press, in press.

——, and G. C. Dodd, 1988: Homogeneous nucleation rate for highly supercooled cirrus cloud droplets. *J. Atmos. Sci.*, **45,** 1357–1369.
——, and B. S. Cho, 1992: Subvisual-thin cirrus lidar dataset for satellite verification and climatological research. *J. Appl. Meteor.*, **31,** 1275–1285.
——, and S. K. Krueger, 1993: Toward an empirical definition of virga: Comments on ''Is virga rain that evaporates before reaching the ground?'' *Mon. Wea. Rev.*, **121,** 2426–2428.
——, R. P. Benson, and J. D. Spinhirne, 2000: Tropical cirrus cloud properties from TOGA/COARE airborne polarization lidar. *Geophys. Res. Lett.*, **27,** 673–676.
Schiffer, R. A., and W. B. Rossow, 1983: The International Satellite Cloud Climatology Project (ISCCP): The first project of the World Climate Research program. *Bull. Amer. Meteor. Soc.*, **64,** 779–784.
Schotland, R. M., K. Sassen, and R. J. Stone, 1971: Observations by lidar of linear depolarization ratios by hydrometeors. *J. Appl. Meteor.*, **10,** 1011–1017.
Starr, D. O'C., and D. P. Wiley, 1990: The 27–28 October 1986 FIRE IFO cirrus case study: Meteorology and clouds. *Mon. Wea. Rev.*, **118,** 2259–2287.
Stephens, G. L., S. Tsay, P. W. Stackhouse Jr., and P. J. Flatau, 1990: The relevance of the microphysical and radiative properties of cirrus clouds to climate and climate feedback. *J. Atmos. Sci.*, **47,** 1742–1753.
Stokes, G. M., and S. E. Schwartz, 1994: The Atmospheric Radiation Measurement (ARM) program: Programmatic background and design of the cloud and radiation testbed. *Bull. Amer. Meteor. Soc.*, **75,** 1201–1221.
Stone, R. G., 1957: A compendium on cirrus and cirrus forecasting. Air Weather Service Tech. Rep. AWS TR 105-130, U.S. Air Force, 156 pp.
Takano, Y., and K.-N. Liou, 1995: Solar radiative transfer in cirrus clouds. Part III: Light scattering by irregular ice crystals. *J. Atmos. Sci.*, **52,** 818–837.
World Meteorological Organization, 1987: *International Cloud Atlas.* Vol. 2, World Meteorological Organization, 212 pp.